

Gravitational Waves from Nonlinear Couplings of Radial and Polar Nonradial Modes in Relativistic Stars

Andrea Passamonti,¹ Nikolaos Stergioulas,¹ and Alessandro Nagar²

¹*Department of Physics, Aristotle University of Thessaloniki, 54124 Thessaloniki, Greece*

²*Dipartimento di Fisica, Politecnico di Torino, Corso Duca degli Abruzzi 24, 10129 Torino, Italy
and INFN, sez. di Torino, Via P. Giuria 1, Torino, Italy*

(Dated: July 15, 2018)

The post-bounce oscillations of newly-born relativistic stars are expected to lead to gravitational-wave emission through the excitation of nonradial oscillation modes. At the same time, the star is oscillating in its radial modes, with a central density variation that can reach several percent. Nonlinear couplings between radial oscillations and polar nonradial modes lead to the appearance of combination frequencies (sums and differences of the linear mode frequencies). We study such combination frequencies using a gauge-invariant perturbative formalism, which includes bilinear coupling terms between different oscillation modes. For typical values of the energy stored in each mode we find that gravitational waves emitted at combination frequencies could become detectable in galactic core-collapse supernovae with advanced interferometric or wide-band resonant detectors.

PACS numbers: 04.30.Db, 04.40.Dg, 95.30.Sf, 97.10.Sj

I. INTRODUCTION

Oscillations of neutron stars can arise in strongly nonlinear phases of stellar evolution, such as during the post-bounce phase in core collapse of massive stars or during the merger of compact binary systems. Linear perturbation theory is appropriate for describing the dominant properties of stellar pulsations, but neglects several interesting nonlinear effects that can modify or enrich the linear description. For instance, a nonlinear approach is required for understanding how energy transfer between various classes of modes could saturate the r- and f-mode instabilities in rotating stellar models (see [1] and references therein), or limit the persistence of the bar-mode instability, through nonlinear coupling between $m = 1$ and $m = 2$ modes [2, 3, 4]. Nonlinear mode couplings also become important in the development of a g-mode instability, that was recently observed in core-collapse simulations [5]. Another nonlinear effect relevant for pulsations in rapidly rotating stars is the mass-shedding-induced damping of pulsations [6, 7].

The main nonlinear effect appearing even for mildly nonlinear pulsations is the presence of combination tones, which are nonlinear harmonics whose frequency appears as a linear combination of linear eigenfrequencies (see [7, 8, 9]). The number of linear terms in the combination tones is equal to the nonlinear order of the mode coupling. In perturbation theory, these nonlinear features can be addressed starting at bilinear order, for the coupling of two linear modes.

The presence of nonlinear harmonics can lead to exchange of energy between modes or even to two-mode or three-mode resonances or parametric instabilities [9]. In rotating proto-neutron stars, rotational effects can increase the number of possible resonances between axisymmetric modes [7]. The parameter space for possible resonances or instabilities is even larger for non-

axisymmetric oscillations. In this case, each l -mode is split in its m components proportionally to the rotation rate of the star. Therefore, at large rotation rates, several modes could satisfy resonance conditions [10].

Gravitational waves emitted by neutron star pulsations are interesting sources for current detectors, but the high-frequency band will only start becoming accessible with the construction of advanced detectors, such as Advanced LIGO [11], VIRGO+ and Advanced VIRGO [12, 13]. There are also plans for detectors with significantly increased sensitivity at several kHz, such as the GEO-HF project [14], and the proposal for the Dual wide-band bar detector [15]. Nonlinear effects in neutron star pulsations could be probed with such instruments.

Interest in the nonlinear dynamics of stellar pulsations exists also for variable stars, such as Cepheids, RR Lyræ and δ Scuti stars. The modulation of the pulsation amplitude (Blazkho effect) or other irregular oscillations, which have been observed in the velocity and light curve of these stars, could be explained by nonlinear interaction between various modes. These studies have been carried out mainly in Newtonian perturbation theory by using amplitude equations (see e.g. [16, 17, 18] and references therein).

General Relativity provides a more appropriate framework for studying compact objects, where relativistic effects, such as the dragging of the inertial frames or the dynamical role of the spacetime, can influence the spectral properties of hydrodynamical modes or introduce new features, such as w -modes [19]. Modern high-resolution methods [20] (in particular, the 3rd-order PPM scheme) implemented in numerical relativity codes, have allowed in recent years the study of nonlinear pulsations in non-rotating and rotating stars (see [6, 7, 21, 22, 23]). The above studies included 2-D and 3-D simulations of axisymmetric modes in either the relativistic Cowling approximation, the spatially conformal flatness (CFC) approximation or full general relativity. Nonlinear rela-

tivistic radial pulsations have also been addressed with a different method in [24, 25], where the nonlinear dynamics was studied as a deviation from an equilibrium background.

Complementary to fully nonlinear approaches, nonlinear perturbative techniques can be very useful in weakly and mildly nonlinear regimes for understanding how a physical process is affected by nonlinear effects. In addition, the dimensional reduction of the problem by separation of variables (when possible) yields a much less computationally expensive approach, suitable for large parameter studies. In order to correctly address the gauge freedom of general relativity, a relativistic perturbation theory has been introduced in [26], and then extended to physical systems where two or more variables can be assumed as perturbative parameters [27, 28, 29]. For spherically symmetric and time dependent spacetimes, a gauge invariant formalism for studying spherical and nonspherical perturbations was introduced by Gerlach and Sengupta [30, 31]. This formalism was further developed in [32, 33] and then extended (with partial gauge-invariance at second and higher perturbative orders) in [34] (from now on GSGM formalism). Efforts are now under way for formulating a fully gauge-invariant theory at second or higher order [34].

Second-order perturbative studies have been carried out in cosmology [35], or for investigating the Schwarzschild [36, 37, 38] and Kerr [39] spacetimes. In the two-parameter relativistic perturbative framework, the coupling between the radial and nonradial oscillations of perfect-fluid, spherically symmetric neutron stars has been recently investigated in [9, 40, 41]. In particular, the coupling between the radial and axial oscillations exhibits an interesting resonance when a radial mode frequency approaches the frequency of an axial w -mode [9, 41].

In this paper, we address the coupling between the radial and polar nonradial modes by numerically solving the perturbation equations introduced in [40] for polytropic, nonrotating relativistic stars. In the polar sector, new interesting results are expected as the spectrum of polar modes is generally richer than the axial case. In particular, we set up initial conditions (in following recent numerical simulations of core collapse [42, 43]) for studying pulsating protoneutron stars. In the post-bounce phase a newly-born neutron star is expected to mainly oscillate in its radial ($l = 0$) and nonradial quadrupole ($l = 2$) modes [42, 43] with a variation in its central density of several percent. After investigating several initial pulsating configurations, we have found that for a 5% variation in the central energy density and about $10^{-7}M_{\odot}$ energy stored in nonradial oscillations some bilinear combination tones are within the sensitivity window of advanced and newly proposed gravitational wave detectors. A possible detection of these combination tones, in addition to the linear modes, would provide new important information for solving the high-density equation of state puzzle through gravitational-wave asteroseismology. Note that the perturbative equations as de-

veloped in [9, 40, 41] do not contain back-reaction terms. This issues is the subject of future work.

The plan of this paper is as follows. Sections II and III are dedicated to the description of the background stellar configuration and the perturbative framework, respectively. The set of perturbed initial data, boundary conditions and main properties of the numerical code are addressed in Sec. IV. In Sec. V, we present the temporal and spectral properties of the fluid and Zerilli variables, which arise from the coupling between radial and polar nonradial oscillations. The detectability of the gravitational wave signal is discussed in Sec. VI. In Appendix A we present the equations that complete the system of nonradial perturbation equations given in [40], while in Appendix B we derive the pulsational kinetic energy of nonradial oscillations in terms of GSGM formalism.

In this paper the geometrical units are adopted, where $G = c = 1$.

II. BACKGROUND EQUILIBRIUM

The background spacetime is the equilibrium configuration of a perfect-fluid spherically symmetric nonrotating star, which is described by the following spacetime metric:

$$ds^2 = -e^{2\Phi} dt^2 + e^{2\Lambda} dr^2 + r^2(d\theta^2 + \sin^2\theta d\phi^2), \quad (1)$$

where $\Phi = \Phi(r)$ and $\Lambda = \Lambda(r)$ are obtained by solving the Tolman-Oppenheimer-Volkov (TOV) equations. This system of equations is closed by an equation of state (EoS) that characterizes the fluid properties. In this paper we consider a relativistic barotropic EoS:

$$p = K\rho^{\Gamma}, \quad (2)$$

$$\varepsilon = \rho + \frac{p}{\Gamma - 1}, \quad (3)$$

where p is the pressure, ρ and ε are the rest mass density and the total energy density respectively, and K and Γ are the polytropic parameters. For a central density $\rho_c = 5.87 \times 10^{-4} \text{ km}^{-2}$ and polytropic parameters $K = 217.858 \text{ km}^2$ and $\Gamma = 2$, the TOV equations provide a stellar model with typical mass $M = 1.40M_{\odot}$ and radius $R = 14.151 \text{ km}$ [7].

III. PERTURBATIVE FRAMEWORK

The system of perturbation equations for studying the coupling between the radial and nonradial oscillations of spherical star has been introduced in [9, 40, 41]. Therefore in this paper we only report the main properties of the perturbation framework and equations. For more details see the references cited above.

The study of linear perturbations of a spherically symmetric background can be significantly simplified by adopting the expansion of the perturbed quantities in

scalar, vector and tensor harmonics. This technique enables us to separate in the perturbed quantities the angular dependence from the time and radial parts. This reduces the problem to just one spatial dimension. Any harmonic component of the linear perturbative variables is then identified by the harmonic indices (ℓ, m) and is dynamically independent. A further sub-classification can be carried out on a spherically symmetric background, where two perturbation classes with opposite parity and independent dynamics can be defined, namely the axial (*odd-parity*) and the polar (*even-parity*) perturbations.

The above perturbative technique can be extended to second order perturbations. However, due the hierarchical structure of the perturbation methods the nonlinear perturbations obey inhomogeneous perturbation equations, where the homogeneous part has the same differential structure as the linear perturbation equations, whereas the source terms are made by the product of linear perturbations. From the form of these quadratic terms, we can notice that the (ℓ, m) second order perturbations depends on self coupling terms, which couple linear perturbations with the same harmonic index ℓ , and mixed terms, which are instead the product of linear perturbations with different harmonic indices.

In this paper as well as in [9, 40, 41], we select the coupling between the radial ($\ell = 0$) and nonradial ($\ell \geq 2$) perturbations, and concentrate on the numerical simulations of the polar perturbative class. For the coupling between the radial and axial nonradial oscillations see [9, 41]. In order to study the gauge properties of the linear and nonlinear perturbations, we have found convenient to use the 2-parameter relativistic perturbation theory [27] and the gauge invariant formalism of Gerlach and Sengupta [30, 31, 32, 33], in the version developed by [32, 33], that we call GSGM formalism. We have labelled the radial and nonradial perturbation with two distinct parameters and studied the gauge invariance of our nonlinear quantities. This particular coupling can then be studied by means of variables that are gauge invariant when the linear radial perturbation gauge is fixed. Adopting the so-called *radial gauge* for the radial perturbations, the problem becomes essentially that of linear polar perturbations on a time-dependent spherical background.

The remainder of this section is dedicated to the description of the main properties of the radial and nonradial perturbations and their coupling terms. We label linear radial quantities by a $(1,0)$ superscript, linear nonradial quantities by a $(0,1)$ superscript and coupling terms by a $(1,1)$ superscript. The radial pulsations are described by a set of four perturbative fields, namely two metric quantities $S^{(1,0)}$, $\eta^{(1,0)}$ and two fluid variables, which are the enthalpy $H^{(1,0)}$ and the velocity $\gamma^{(1,0)}$ variables. They obey three first order in time evolution equations and two constraints, as there is a single radial degree of freedom. We can then solve a hyperbolic-elliptic system of equations, which is formed by two hyperbolic equations, for $\gamma^{(1,0)}$ and $H^{(1,0)}$, and the Hamiltonian con-

straint that at any time step updates the variable $S^{(1,0)}$, while $\eta^{(1,0)}$ is determined by the second elliptic equation.

The linear polar nonradial oscillations can be studied with a set of gauge invariant quantities [32, 33, 40], the three metric perturbations $S^{(0,1)}$, $k^{(0,1)}$, $\psi^{(0,1)}$ and the three fluid variables $H^{(0,1)}$, $\gamma^{(0,1)}$, $\alpha^{(0,1)}$. Among the different systems of perturbation equations that are available in the literature, we choose a system of three partial differential equations for the three variables $S^{(0,1)}$, $k^{(0,1)}$ and $H^{(0,1)}$. It consists of two hyperbolic equations, which describe respectively the gravitational waves and sound waves propagations, and an elliptic equation, i.e the Hamiltonian constraint [9, 44, 45]. Since the Hamiltonian constraint is used for updating at any time step one of the unknowns of the problem, the errors associated with the violation of this constraint are corrected. The other nonradial variables $\psi^{(0,1)}$, $\gamma^{(0,1)}$, $\alpha^{(0,1)}$, which are necessary for updating the source terms of the second order perturbative equations, can be obtained by three hyperbolic partial differential equations that are reported in Appendix A.

The nonlinear coupling terms obey the same system of equations as the linear nonradial terms, but with nonvanishing source terms in the region interior to the star. Therefore, we evolve the two metric quantities $S^{(1,1)}$ and $k^{(1,1)}$ and the fluid variable $H^{(1,1)}$. In order to understand the structure of the perturbative framework we define the following set of linear and nonlinear perturbations:

$$\mathcal{R}^{(1,0)} \equiv \left(S^{(1,0)}, \eta^{(1,0)}, H^{(1,0)}, \gamma^{(1,0)} \right), \quad (4)$$

$$\mathcal{N}^{(0,1)} \equiv \left(S^{(0,1)}, k^{(0,1)}, \psi^{(0,1)}, H^{(0,1)}, \gamma^{(0,1)}, \alpha^{(0,1)} \right), \quad (5)$$

$$\mathcal{Q}^{(1,1)} \equiv \left(S^{(1,1)}, k^{(1,1)}, H^{(1,1)} \right), \quad (6)$$

and write the system of the three perturbative equations for the coupling as follows:

$$\mathbf{L}_{NR} \left[\mathcal{Q}^{(1,1)} \right] = \mathbf{S} \left[\mathcal{R}^{(1,0)} \otimes \mathcal{N}^{(0,1)} \right], \quad (7)$$

where \mathbf{L}_{NR} is an operator representing the homogeneous part of the system, which has the same differential structure as the linear nonradial perturbation equations for the variables $S^{(1,1)}$, $k^{(1,1)}$ and $H^{(1,1)}$. The source terms are instead represented by the operator \mathbf{S} , which also contains spatial and first order time derivatives.

Outside the star, the linear polar nonradial perturbations have just one degree of freedom, which is described by means of the Zerilli-Moncrief function [46]. In terms

of the gauge-invariant variables it is given by ¹

$$Z^{(0,1)} = \frac{4r^2 e^{-2\Lambda}}{\ell(\ell+1)[(\ell(\ell+1)-2)r+6M]} \left[rS^{(0,1)} + \frac{1}{2} \left(\ell(\ell+1) + \frac{2M}{r} \right) e^{2\Lambda} k^{(0,1)} - r k_{,r}^{(0,1)} \right], \quad (8)$$

where M is the mass of the star. The radial-nonradial coupling terms have the same angular dependence and satisfy an equivalent Zerilli-Moncrief wave-like equation as the linear nonradial perturbation. We denote this variable as $Z^{(1,1)}$; it is constructed from an expression of the form of Eq. (8) with all the variables of type $^{(0,1)}$ replaced by the corresponding $^{(1,1)}$ ones. For any multipole (ℓ, m) , the total Zerilli-Moncrief function is obtained as

$$Z_{\ell m} \equiv Z \equiv Z^{(0,1)} + Z^{(1,1)}, \quad (9)$$

where we have explicitly reintroduced the multipolar indices. As a result, the total emitted power in gravitational radiation (at infinity) is computed as (see for example [47])

$$\frac{dE}{dt} = \frac{1}{64\pi} \sum_{\ell \geq 2, m} \frac{(\ell+2)!}{(\ell-2)!} |\dot{Z}_{\ell m}|^2, \quad (10)$$

where the overdot denotes time derivative.

IV. SETTING UP NUMERICAL SIMULATIONS

The numerical code for studying the dynamical evolution of polar coupling perturbations has the same structure as the code developed in [9, 41] for the axial coupling case. We had to replace the parts of the code that compute the axial linear and coupling perturbations with the new routines that are appropriate for the polar sector. For details about the overall structure of the code see [9, 41], while for the part that solves the polar nonradial perturbations see [44, 45]. This latter part has also been used for treating the equations for the radial-nonradial terms, by adding the source terms found in [40, 41].

A. Initial Data

The independence of linear perturbations from the harmonic index ℓ implies that we need to separately excite the radial and nonradial oscillations. In order to simplify the study of numerical simulations and identify the

TABLE I: Eigenfrequencies (in kHz) of the first eight fluid modes of the radial and nonradial $\ell = 2$ polar perturbations. The second column corresponds to the results from calculation in the frequency domain (the solution of the Sturm-Liouville problem [9]), while the third column displays the results of an FFT of the enthalpy time evolution. In square brackets we denote the relative difference between the frequencies extracted from the time evolution and the Sturm-Liouville solutions. The fourth column shows the frequencies of the polar nonradial oscillations, which are determined by an FFT of a time-domain simulation.

Radial	Freq. code	FFT	Nonradial	FFT
F	1.443	1.437 [0.4%]	² f	1.587
H ₁	3.955	3.951 [0.1%]	² p ₁	3.757
H ₂	5.916	5.913 [0.05%]	² p ₂	5.699
H ₃	7.775	7.771 [0.05%]	² p ₃	7.614
H ₄	9.590	9.587 [0.03%]	² p ₄	9.419
H ₅	11.38	11.368 [0.1%]	² p ₅	11.25
H ₆	13.15	13.152 [0.01%]	² p ₆	13.03
H ₇	14.92	14.916 [0.02%]	² p ₇	14.781

correct nonlinear harmonics we have excited the linear perturbations by selecting specific modes. For radial pulsations we have set up a Sturm-Liouville problem for the radial velocity perturbations and solved it numerically with relaxation methods. As tested in [9, 41], this code determines the eigenfrequencies of radial modes with an accuracy to better than 0.2% with respect to the published values. With an appropriate choice of the initial phases for the various perturbed variables, we can excite the radial eigenmodes by providing only the eigenfunctions associated with the radial velocity perturbation $\gamma^{(1,0)}$. The simulations are numerically stable over a large multiple of the largest oscillation period that we are interested in. Using Fast Fourier Transformations (FFT) of the time evolution of selected variables, we can reproduce the linear mode frequencies of radial modes with an accuracy to better than 0.4%, as shown in Table I. More details can be found in [9, 41].

There are various sets of initial conditions for exciting the polar nonradial perturbations which satisfy the Hamiltonian and momentum constraints on the initial slice [44, 48, 49]. After having explored all the different choices mentioned in the literature, we have not noticed any important qualitative difference with respect to the coupling perturbations. Therefore, in this paper we consider only a representative case, which consists in perturbing the fluid with an enthalpy eigenfunctions, imposing $S^{(0,1)} = 0$ (conformally flat initial data) and determining $k^{(0,1)}$ by solving the Hamiltonian constraint.

The enthalpy eigenfunctions are obtained with the *eigenfunction recycling* method developed in [6, 7], where the eigenfunction is extracted after a simulation by means of FFT transformations at every grid point. In a first

¹ In the reference [40] there is a typo in the definition of the Zerilli-Moncrief function that here we have corrected. In the same paper, equation (79) must be corrected as follows: $U = u^A v_A = \lambda \frac{e^{-\Lambda}}{r} \gamma^{(1,0)}$.

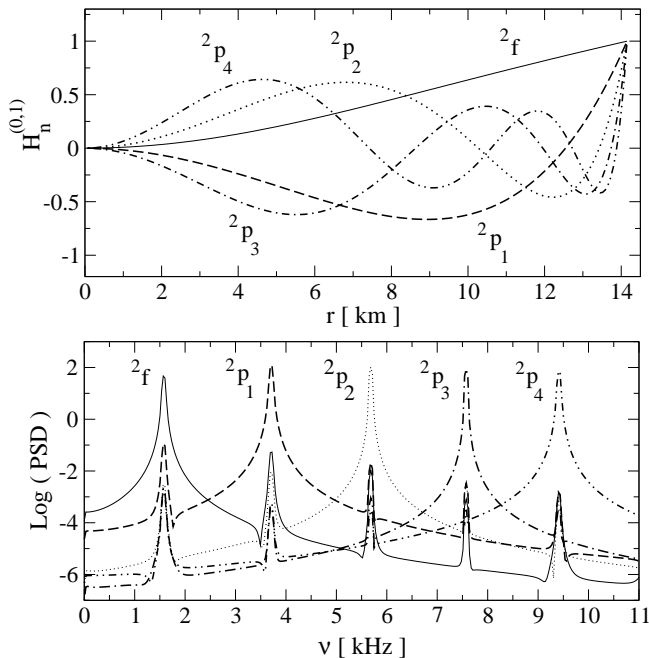


FIG. 1: Normalized eigenfunctions of the perturbed enthalpy for the fundamental nonradial mode 2f and its first four overtones, 2p_1 to 2p_4 (*upper panel*). The *lower panel* displays the Fourier power spectral density of the evolution of the perturbed enthalpy, in simulations where each of the above eigenfunctions was used as an initial perturbation. In all cases, the desired mode is predominantly excited, while other modes (still excited due to truncation errors) have an amplitude which is several orders of magnitude smaller.

simulation, we use trial eigenfunctions that excite various modes. The eigenfunction of the desired mode is then extracted and used as an initial perturbation for a second simulation, in which case the desired mode is predominantly excited. This *recycling* procedure can be repeated until the amplitude of the other modes becomes sufficiently small. Examples of extracted eigenfunctions are shown in the top panel of Fig. 1, which displays the eigenfunctions of the fundamental quadrupole mode 2f and its first four overtones 2p_1 to 2p_4 , for the equilibrium model mentioned in Sec. II. The lower panel displays the Fourier power spectral density (PSD) of the time evolution of the perturbed enthalpy, in simulations where each of the above eigenfunctions was used as an initial perturbation. In all cases, we observe that the desired mode is predominantly excited, while other modes (still excited due to truncation errors) have an amplitude which is several orders of magnitude smaller.

B. Case Studies

The nonlinear coupling between radial and nonradial modes is studied here in a number of particular cases, in which the perturbed initial data consists of a linear

TABLE II: Initial configurations (CASE I – IV), constructed by various linear combinations of eigenfunctions corresponding to particular radial and nonradial modes. For the relative amplitudes used in these linear combination, see the main text.

CASE	Radial modes	Nonradial modes
I	F	2f
II	F, H_1, H_2, H_3, H_4, H_5	2f
III	F	${}^2f, {}^2p_1, {}^2p_2, {}^2p_3, {}^2p_4, {}^2p_5$
IV	F, H_1, H_2, H_3, H_4, H_5	${}^2f, {}^2p_1, {}^2p_2, {}^2p_3, {}^2p_4, {}^2p_5$

combination of various radial and (quadrupole) nonradial modes. Table II provides a summary of the modes used in each case. In CASE I, only the fundamental radial and the fundamental nonradial modes are present in the perturbed initial data. CASE II includes, in addition, the first five radial overtones. CASE III includes the fundamental radial and nonradial modes plus the first five nonradial overtones. Finally, CASE IV includes all radial and nonradial modes up to the fifth overtone.

The amplitude of each linear mode is determined by choosing a particular value of its pulsational kinetic energy. For radial pulsations, the kinetic energy is computed at an instant of vanishing Lagrangian displacement (vanishing potential energy, maximum kinetic energy) as [50]:

$$E_k^{(1,0)} = 2\pi \int_0^R dr (\varepsilon + p) e^{\Lambda+\Phi} \left(r \gamma^{(1,0)} \right)^2, \quad (11)$$

where $\gamma^{(1,0)}$ is related to the perturbed radial velocity.

For nonradial pulsations, the kinetic energy can be determined in terms of the GSGM quantities in the Regge-Wheeler gauge as follows (see Appendix B):

$$E_k^{(0,1)} = \frac{1}{2} \int_0^R dr (\varepsilon + p) e^{\Phi+\Lambda} \left[r^2 \left(\gamma^{(0,1)} - \frac{\psi^{(0,1)}}{2} \right)^2 + \ell(\ell+1) \left(\alpha^{(0,1)} \right)^2 \right], \quad (12)$$

where $\gamma^{(0,1)}$ and $\alpha^{(0,1)}$ are proportional to the radial and longitudinal components of the velocity, respectively, while the metric perturbation $\psi^{(0,1)}$ is proportional to δg_{r0} . In order to determine the amplitudes of the initial data, we average the pulsational kinetic energy of Eqs. (11)-(12) over several oscillation periods.

After having determined the required amplitude for each mode to get a certain pulsation energy, the radial pulsations are excited by a linear combination of the variables $\gamma_n^{(1,0)}$ (related to the radial velocity eigenfunction), where the index n denotes different modes:

$$\gamma^{(1,0)} = \sum_n \gamma_n^{(1,0)}. \quad (13)$$

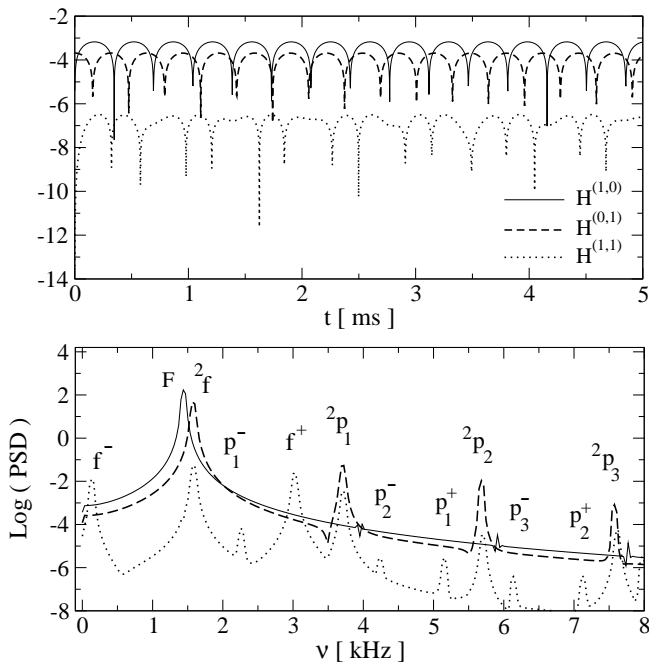


FIG. 2: Time evolution (*upper panel*) and the spectral properties (*lower panel*) of the enthalpy for CASE I, when the star is oscillating at first perturbative order in the radial and nonradial fundamental modes. In the (*upper panel*), the enthalpy is given as $\log |H^{(i,j)}|$, where $i, j = 0, 1$. The radial $H^{(1,0)}$ and nonradial $H^{(0,1)}$ enthalpy are shown with *solid* and *dashed lines* respectively, while $H^{(1,1)}$ is represented with a *dotted line*. The nonlinear harmonics have been denoted as $f^\pm = 2f \pm F$ and $p_n^\pm = 2p_n \pm F$.

Correspondingly, for nonradial oscillations, the linear combination of the enthalpy eigenfunctions $H_n^{(0,1)}$, used to initiate the pulsations, is given by

$$H^{(0,1)} = \sum_n H_n^{(0,1)}. \quad (14)$$

For simplicity we consider vanishing initial data for all coupling variables, i.e. $Q^{(1,1)} = 0$. The Hamiltonian and momentum constraints are then violated on the initial Cauchy hypersurface and the numerical solutions will be effected by an initial transient of short duration [9, 41]. This initial transient is not affecting the main results presented here.

C. Boundary Conditions

To complete the description of the initial-value problem, one needs to impose the boundary conditions at the origin, the stellar surface and at infinity. This topic has been addressed in detail in [9, 40, 41] and hence we do not repeat it here. However, it is worth mentioning that the surface treatment used in the axial case [9, 41] has

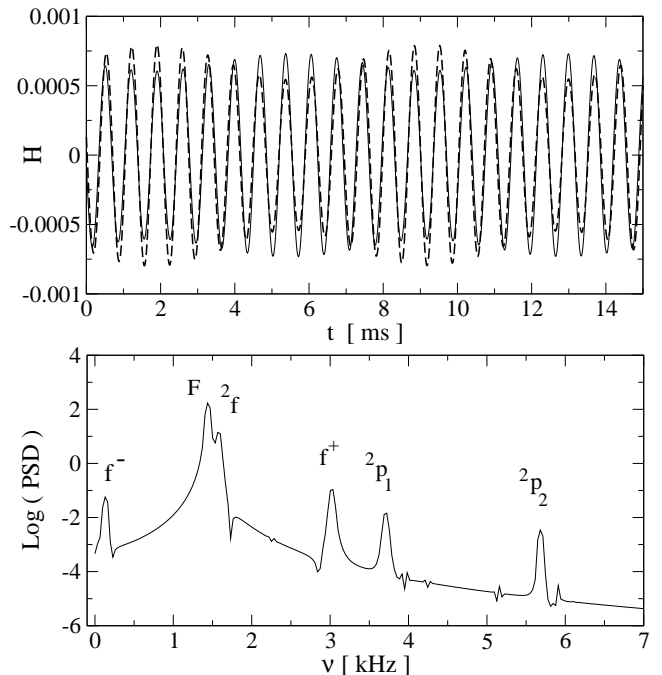


FIG. 3: For the same initial pulsating configuration of Fig. 2 (CASE I) the *upper panel* depicts the total enthalpy H as given by Eq. (15) in the equatorial plane ($\theta = \pi/2$, *solid line*) and in the polar direction ($\theta = 0$, *dashed line*). *Lower panel*: the Fourier power spectral density of H in the equatorial plane.

been also implement for polar modes. During the evolution, some of the junction conditions for the coupling variables could not be correctly imposed, due to the motion of the perturbed stellar surface (see [9, 24]). We address this issue as follows: i) at the stellar surface, we determine the maximal Lagrangian displacement of the linear oscillations and ii) we impose the junction conditions for the coupling variables on a hypersurface which is always inside the oscillating star. This method is equivalent to removing a thin outer layer close to the stellar surface, with a thickness depending on the pulsation amplitude. In practice, for small-amplitude pulsations, only very few grid points near the stellar surface of the equilibrium model need to be neglected for the coupling variables. This does not have a noticeable quantitative effect on our main results.

V. RADIAL-NONRADIAL MODE COUPLINGS

We discuss now the numerical results for the coupling of radial and nonradial pulsations, for the specific cases of initial configurations described in Sec. IV B. In order to interpret the numerical simulations, we first describe the main properties that we expect from the structure of the equations for the coupling perturbative terms $Q^{(1,1)}$. The *linear* radial oscillations will contain the eigenfrequencies

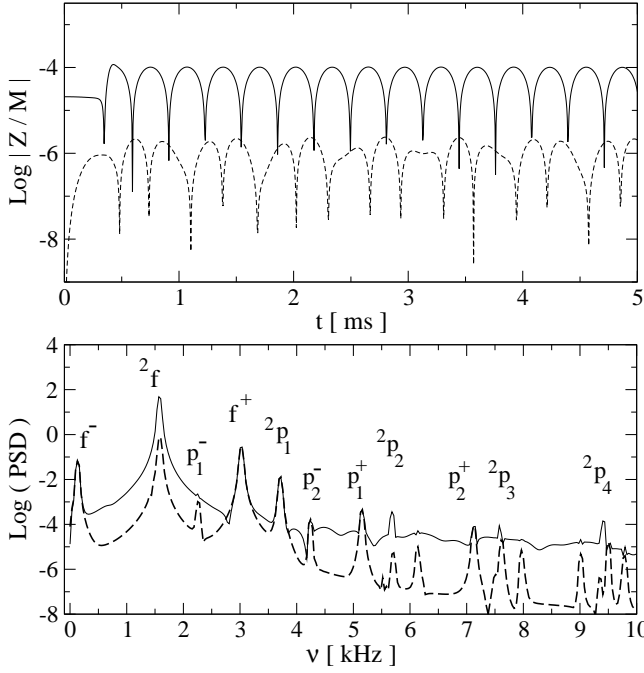


FIG. 4: Gauge-invariant waveforms (*top panel*) and Fourier power spectral density (*bottom panel*) for CASE I: we show together the coupling Zerilli-Moncrief function $Z^{(1,1)}$ (*dashed line*) and the total one $Z \equiv Z^{(0,1)} + Z^{(1,1)}$ (*solid line*).

cies $\nu_i^{(1,0)}$ of the particular radial modes excited by the initial data. Similarly, the *linear* nonradial oscillations, will contain the frequencies $\nu_i^{(0,1)}$ of the particular nonradial modes. The variables describing the radial-nonradial coupling terms, $\mathcal{Q}^{(1,1)}$, which obey equations (7), will then be driven by two different kinds of frequencies: i) the natural frequencies $\nu_n^{(0,1)}$, associated with the homogeneous part of the nonradial equation (7), which are now excited by the forcing term \mathcal{S} , and ii) the nonlinear coupling frequencies, the so-called combination tones, whose frequencies are linear sums or differences of linear mode frequencies. For the second-order coupling between radial and nonradial oscillations, an example of such a combination frequency is $\nu^{(1,1)\pm} = \nu^{(1,0)} \pm \nu^{(0,1)}$.

A. Case I

In CASE I, only the fundamental radial and the fundamental $\ell = 2$ nonradial modes are present in the perturbed initial configuration. In order to set the amplitude of each mode, we take into account recent numerical simulations (see [42, 43, 51, 52, 53] and references therein) which suggest that over a total simulation time of about 20 ms the total energy emitted in gravitational waves can be of order $10^{-8} M_\odot$. Furthermore, the post-bounce radial pulsations in the above simulations induced a variation in the central energy density of the order of 1-5%.

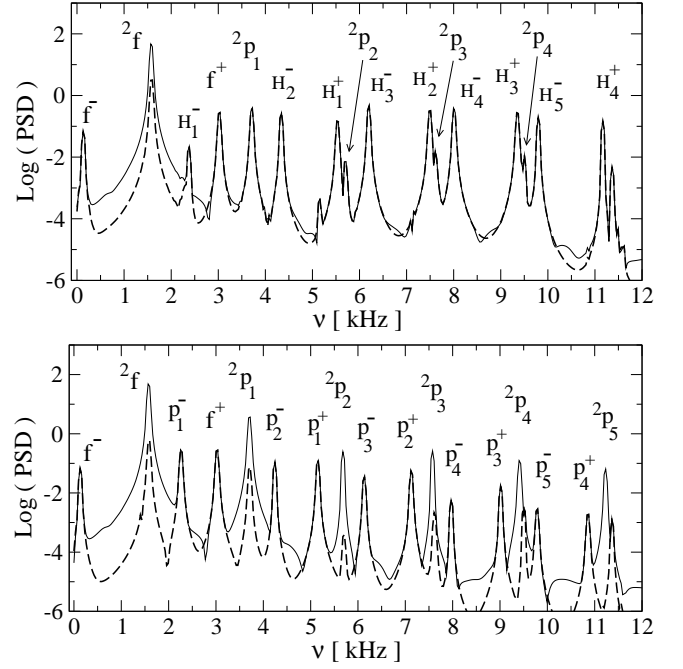


FIG. 5: Fourier power spectral density of $Z^{(1,1)}$ (*dashed line*) and of Z (*solid line*). The *top panel* refers to CASE II and the *lower panel* to CASE III (see text for details). In order to simplify the labelling of the figure we have defined $H_n^\pm = H_n \pm 2f$, $f^\pm = 2f \pm F$ and $p_n^\pm = 2p_n \pm F$.

In our numerical simulations, we find that a gravitational wave energy of $1.11 \times 10^{-8} M_\odot$ (as determined by time integration of Eq. (10)) is emitted after 20 ms of continuous monochromatic emission of the fundamental $\ell = 2$ mode, when the latter has an average kinetic energy of $\langle E_k^{(0,1)} \rangle = 5.0 \times 10^{-8} M_\odot$. In practice, we stop our simulation at 34 ms, so that the energy emitted in gravitational waves is $1.74 \times 10^{-8} M_\odot$. The radial pulsations are excited with an amplitude that corresponds to an average kinetic energy $\langle E_k^{(1,0)} \rangle = 5.0 \times 10^{-7} M_\odot$, which leads to a variation in the central energy density of 1%.

The upper panel of Fig. 2 displays the time evolution of the enthalpy variables $H^{(1,0)}$, $H^{(0,1)}$ and $H^{(1,1)}$ averaged at any time step along the spatial coordinate. While the two linear variables are nearly perfectly monochromatic, the bilinear term $H^{(1,1)}$ contains several frequencies. In the PSD of $H^{(1,1)}$, shown in the lower panel of Fig. 2, several combination frequencies, such as $f^\pm = 2f \pm F$ and $p_n^\pm = 2p_n \pm F$, for $n = 1, 2, 3$, can be clearly identified. We have also verified that the amplitude of $H^{(1,1)}$ is nearly the product of the two oscillation amplitudes of $H^{(1,0)}$ and $H^{(0,1)}$. The top panel of Fig. 3 shows the corresponding time evolution of the (averaged) total enthalpy H (at $\theta = \pi/2$, solid line, and $\theta = 0$, dashed line) defined as

$$H \equiv H^{(1,0)} + \sqrt{\frac{5}{\pi}} \frac{3 \cos^2 \theta - 1}{4} \left(H^{(0,1)} + H^{(1,1)} \right), \quad (15)$$

where the normalization constant of the spherical harmonic Y^{00} is contained in the radial variable $H^{(1,0)}$. One can notice a modulation of the amplitude, which is mainly due to the different angular dependence of the radial and nonradial oscillations. The lower panel of Fig. 3 shows the PSD of H at $\theta = \pi/2$. Both linear radial and nonradial fundamental modes are present. Of the several combination frequencies present in $H^{(1,1)}$, only $f^\pm = 2f \pm F$ have a large enough amplitude to be clearly visible here. We recall that the two lowest-order linear pressure mode frequencies seen in the lower panels of Fig. 2 and Fig. 3 are present because the initial data for the linear fundamental radial mode are not perfect, but also contain additional frequencies with very small amplitudes. The top panel of Fig. 4 shows the time evolution of $Z^{(1,1)}$ (dashed line) and Z (solid line) extracted at $r = 100$ km. We note that the bilinear function $Z^{(1,1)}$ is about two order of magnitude smaller than Z . In the lower panel of the same figure, the corresponding PSD are displayed. The main combination frequencies are $f^\pm = 2f \pm F$, whose detectability will be addressed in Sec. VI below.

B. Cases II and III

Next, we study two initially pulsating configurations where several modes are contemporarily excited. In CASE II, we excite the nonradial fundamental mode $2f$ and a linear combination of radial modes up to the fifth overtone. In CASE III, we excite the radial fundamental mode F and a up to the fifth pressure nonradial mode. The pulsation amplitudes of the two fundamental modes F and $2f$ have the same value as in CASE I. For the overtones, we assume that the kinetic energy decreases proportionally with the order of the mode. This assumption is motivated by the spectral properties of the gravitational waves emitted in core collapse simulation. In particular, we demand that each overtone or pressure mode of order n has one fifth of the energy stored in the $n - 1$ mode; i.e.,

$$\langle E_k^{(1,0)} \rangle_{H_n} = \frac{1}{5} \langle E_k^{(1,0)} \rangle_{H_{n-1}}, \quad (16)$$

$$\langle E_k^{(0,1)} \rangle_{2p_n} = \frac{1}{5} \langle E_k^{(0,1)} \rangle_{2p_{n-1}}, \quad (17)$$

where for $n = 0$ the F and $2f$ modes are implied. Notice that due to phase-cancellations, the total energy, when exciting several modes, is not a linear sum of the individual energies. Using Eq. (11) and Eq. (12) for the total perturbation, we determined that when the radial or nonradial oscillations are excited up to the fifth overtone, the radial and nonradial average kinetic energies are $\langle E_k^{(1,0)} \rangle = 6.25 \times 10^{-7} M_\odot$ and $\langle E_k^{(0,1)} \rangle = 6.0 \times 10^{-8} M_\odot$ respectively.

For CASE II, the upper panel of Fig. 5 displays the PSD of the bilinear Zerilli-Moncrief function $Z^{(1,1)}$ as

well as that of the total Z . On the other hand, the bottom panel of the same figures exhibits the same information for CASE III. The spectra clearly show the presence of several expected combination frequencies: in particular, for CASE III, a repetitive triplet structure (such as, e.g. p_1^+, p_2, p_3^-) is evident in the plot.

Although we have chosen to show only a few representative cases, the bilinearity of all coupling variables is well reproduced by our numerical results. It is therefore trivial to scale our results to any other desirable values of the radial and nonradial average kinetic energies.

VI. GRAVITATIONAL WAVES

In order to assess the detectability of gravitational waves emitted at combination frequencies, when several oscillation modes are present, we focus on CASE IV of Table II, where the fundamental radial and nonradial modes are present together with their first five overtones. The average kinetic energy in the fundamental modes is given as in Sec. VB with the energy in the overtones given again by Eq. (16) and Eq. (17). We also vary the average kinetic energy in the radial modes, between a minimum value $\langle E_k^{(1,0)} \rangle = 6.25 \times 10^{-7} M_\odot$, that results in a central energy density variation of 1%, and a maximum value $\langle E_k^{(1,0)} \rangle = 9.96 \times 10^{-6} M_\odot$, that results in a central energy density variation of 5%. We compute the *characteristic* strain of gravitational waves, defined as in [54]

$$h_c(\nu) \equiv \frac{\sqrt{2}}{\pi d} \sqrt{\frac{dE}{d\nu}}, \quad (18)$$

where $dE/d\nu$ is the energy spectrum of the gravitational signal and d is the distance of the source. The energy spectrum can be written as [47]

$$\frac{dE}{d\nu} = \frac{\pi}{8} \sum_{\ell \geq 2} \frac{(\ell + 2)!}{(\ell - 2)!} \nu^2 |\hat{Z}_{\ell m}|^2, \quad (19)$$

where $\hat{Z}_{\ell m}$ denotes the Fourier transform of the (total) Zerilli-Moncrief function given by Eq. (9). For $\ell = 2$, we have

$$h_c(\nu) = \sqrt{\frac{6}{\pi}} \frac{\nu}{d} |\hat{Z}_{20}|. \quad (20)$$

Figure 6 shows $h_c(\nu)$ for a source at the galactic distance $d = 10$ kpc with an initial oscillating configuration given by CASE IV and for an emission time of 34 ms. On top of this, Fig. 6 also displays the optimal rms noise, $h_{\text{rms}}(\nu)$ for several planned detectors: the interferometric advanced LIGO [11], the advanced VIRGO [12, 13], the GEO-HF [14] designs and the proposed wide-band dual resonant detector Dual SIC [15]. We recall that the optimal rms noise is defined as

$$h_{\text{rms}}(\nu) \equiv \sqrt{S_h \nu}, \quad (21)$$

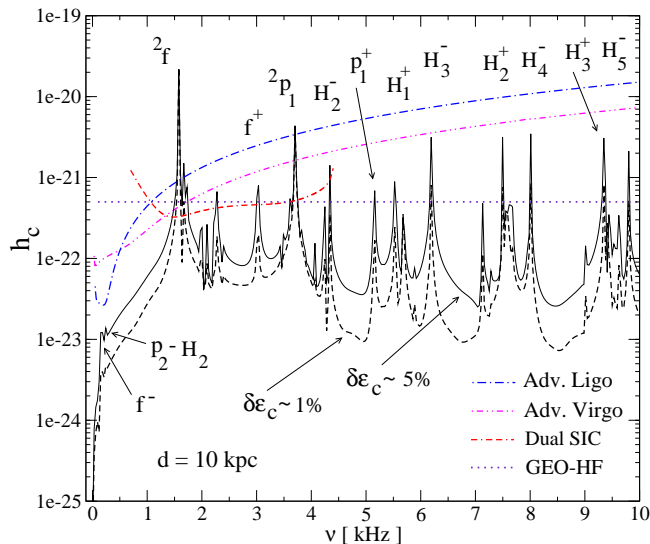


FIG. 6: For a galactic source ($d = 10$ kpc), the figure displays the characteristic strain $h_c(\nu)$ of two initial pulsating configurations for CASE IV of Table II. In the first (*dashed line*) and second (*solid line*) configuration, the radial pulsations respectively lead to 1% and 5% variation of the central energy density. The figure also shows the $h_{\text{rms}}(\nu)$ strain sensitivity, Eq. (21), of AdvLIGO, AdvVIRGO, Dual SIC and GEO-HF detectors (see legend). Some of the linear and bilinear harmonics are within the sensitivity window of these detectors, especially in the $\delta\epsilon_c \sim 5\%$ case.

where $S_h(\nu)$ is the spectral density of the detector strain noise. For signals with random direction and random orientation with respect to the detector, the rms noise should be increased by a factor of $\sqrt{5}$ [54].

Of the several linear nonradial modes excited in the simulation for CASE IV, only the two lowest-order ones, 2f and 2p_1 have a characteristic amplitude above the rms noise of either Advanced LIGO (AdvLIGO) or Advanced VIRGO (AdvVIRGO). When a 1% central density variation for the radial oscillations is assumed, then all bilinear combination frequencies are also below the strain sensitivity, for the above two detectors. However, when a 5% central density variation for the radial oscillations is assumed, then some bilinear combination frequencies are above the rms noise of either AdvVIRGO or both AdvLIGO and AdvVIRGO.

For the GEO-HF detector, a large number of bilinear harmonics is above the strain sensitivity curve at a 5% central density variation of radial oscillations. With such a detector, even harmonics of up to 10 kHz could become detectable. At the lower limit of a 1% central density variation, some bilinear harmonics have a characteristic amplitude which is marginally above the strain sensitivity curve.

Figure 7 focuses on the 1 to 2.5 kHz region of Fig. 6. The detectable bilinear combination frequencies are close to the frequency of the fundamental 2f mode. Specifically, the ${}^2p_3 - H_2$ and the ${}^2p_4 - H_3$ combination fre-

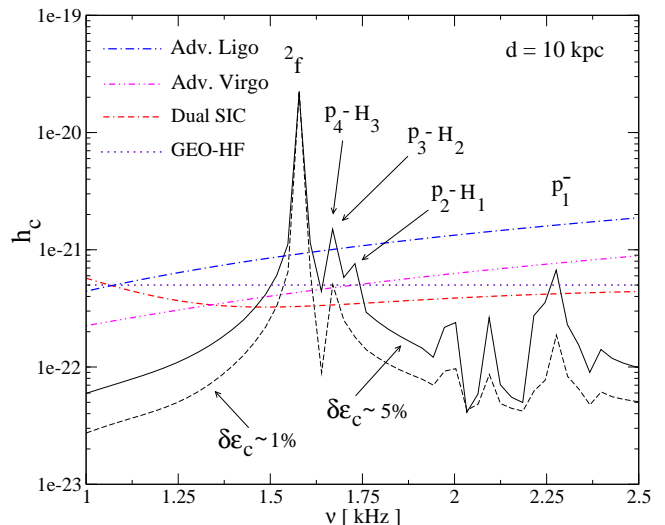


FIG. 7: Blow up of Fig. 6 in the region where the chance of a detection is higher. Besides the linear 2f and 2p_1 modes, there are several combination tones with a characteristic strain larger than the detector noise, in particular for the $\delta\epsilon_c \sim 5\%$ configuration. Note that the combination tones $p_3 - H_2$ and $p_4 - H_3$ fall into the same frequency bin and then are indistinguishable.

quencies fall into the same frequency bin and their combined amplitude exceeds the noise curve for both the AdvLIGO and AdvVIRGO detectors, for a 5% central density variation. It is thus apparent, that some bilinear combination frequencies may be interesting even for the AdvLIGO or AdvVIRGO designs. For the Dual SIC detector design, several bilinear harmonics fall within its sensitivity window in the range of up to 4.5 kHz. Figure 7 shows that the ${}^2p_4 - H_3$ harmonic could become detectable even at a 1% central density variation. Higher signal-to-noise ratios and better event rates can be achieved with more advanced designs, such as the design for the EURO detector in xylophone mode [55].

VII. DISCUSSION

Using a gauge-invariant perturbative formalism, we studied the bilinear coupling between the radial and non-radial polar pulsations in a relativistic star. For typical values of mode-energies expected in the post-bounce phase of core-collapse supernovae, we find that some bilinear combination frequencies may become detectable with planned interferometric detectors, such as Advanced VIRGO and GEO-HF, or with proposed wide-band resonant detectors, such as the Dual SIC.

The possible detection of bilinear combination frequencies, in addition to the expected linear mode frequencies, would yield significant new constraints for the high-density equation of state of compact stars, as they also contain information on the radial modes of the star. Us-

ing empirical relations constructed for gravitational-wave asteroseismology [56, 57, 58], in combination with numerical data for radial modes in realistic compact-star models [59] could allow for the determination of both the mass and radius of the star with good accuracy.

Bilinear combination frequencies of rotating proto-neutron stars were recently studied in [7] where it was found that rotational changes result in the difference in frequency between two overtones coming close to the frequency of a fundamental mode. For such cases it was suggested that these crossings could result in an enhanced gravitational-wave emission at the combination frequencies, due to 3-mode resonances. The results presented here possibly allows for such an interpretation, as the amplitude of the ${}^2p_3 - H_2$ and ${}^2p_4 - H_3$ frequencies in Fig. 7, is larger than the amplitude of the ${}^2p_2 - H_1$ frequency. Since the latter involves modes of lower order (and of higher average kinetic energy in our examples), one would expect the opposite result. It is thus possible that the amplitude at the ${}^2p_3 - H_2$ and ${}^2p_4 - H_3$ frequencies is larger because of a resonance effect with the linear 2f mode. Although we have not included back-reaction effects, the imprint of a possible resonance may be already present in the structure of the equations at the bilinear order that is treated here.

In the present work, we have only focused on one particular, cold equilibrium model. In a follow-up study, we will survey a larger number of equilibrium modes and examine the dependence of the detectability of bilinear harmonics in gravitational waves on the equation of state and the compactness of the star. In a more realistic study, the influence of the high entropy immediately after core bounce, the subsequent thermal evolution of the equilibrium model and rotational and magnetic-field effects should also be taken into account. In addition, numerical simulations have shown that significant mass accretion onto the proto-neutron star (PNS), the settling of the PNS to smaller radii (factor of 2) and a non-negligible density in the PNS hot envelope, all contributes to the gravitational wave signal between the end of the initial phase of bounce ring down (~ 10 ms post bounce) and the start of convection in the hot bubble (~ 70 ms post bounce) [51]. When additional factors are taken into account, our perturbative study could help in resolving specific features in the complex gravitational wave signal in realistic core-collapse.

In another study, we are planning on using amplitude equations in perturbation theory and a fully nonlinear numerical code, as in [7], to also explore possible saturations of the nonlinear oscillations or the existence of possible resonances or parametric instabilities, as suggested in [7, 9, 40].

Acknowledgments: We thank Marco Bruni, Massimo Cerdonio, Harry Dimmelmeier, Leonardo Gualtieri, Michele Punturo, Carlos Sopuerta, Kostas Kokkotas and

Ewald Müller for fruitful discussions and comments on the manuscript. We are grateful to Massimo Cerdonio and Michele Bonaldi for providing the sensitivity curve for the Dual SIC bar detector and to Michele Punturo for the sensitivity curve of Advanced VIRGO. A.P. is supported by a “Virgo EGO Scientific Forum (VESF)” grant and by the EU program ILIAS.

APPENDIX A: NONRADIAL PERTURBATION EQUATIONS

In this section, we write the perturbation equations for some of the linear nonradial perturbations of a nonrotating spherical star, i.e. the metric variable $\psi^{(0,1)}$, and the velocity $\gamma^{(0,1)}$ and $\alpha^{(0,1)}$. In fact, the closed system of perturbation equations for the enthalpy $H^{(0,1)}$ and the two metric quantities $S^{(0,1)}$ and $k^{(0,1)}$ is already given in [40, 41].

$$\psi_{,t}^{(0,1)} = -2\Phi_{,r} e^{\Phi-\Lambda} \left(rS^{(0,1)} + k^{(0,1)} \right) - e^{\Phi+\Lambda} \left(rS^{(0,1)} \right)_{,r}, \quad (\text{A1})$$

$$\gamma_{,t}^{(0,1)} = -\Phi_{,r} \left(rS^{(0,1)} + k^{(0,1)} \right) - H_{,r}^{(0,1)} + \frac{1}{2} k_{,r}^{(0,1)}, \quad (\text{A2})$$

$$\alpha_{,t}^{(0,1)} = \left[\frac{1}{2} \left(rS^{(0,1)} + k^{(0,1)} \right) - H^{(0,1)} \right] e^{\Phi}, \quad (\text{A3})$$

where from one of the TOV equation we have:

$$\Phi_{,r} = \left(4\pi p r + \frac{m}{r^2} \right) e^{2\Lambda}. \quad (\text{A4})$$

APPENDIX B: PULSATONAL KINETIC ENERGY

The kinetic pulsation energy can be determined as in [60], that in terms of the GSGM variables is given by

$$E^{(0,1)} = \frac{1}{2} \int_0^R dr (\varepsilon + p) \delta u_i \delta u^i e^{\Phi} \sqrt{{}^3g} d^3x, \quad (\text{B1})$$

where $d^3x = dr d\theta d\phi$ and 3g is the determinant of the 3-metric. The covariant 3-velocity of the nonradial perturbations is instead given by the following expression:

$$\delta u_i = \left(\left(\tilde{\gamma}^{(0,1)} - \frac{\psi^{(0,1)}}{2} \right) e^{\Lambda} Y^{lm}, \tilde{\alpha}^{(0,1)} Y_{,\theta}^{lm}, 0 \right), \quad (\text{B2})$$

where $\tilde{\gamma}^{(0,1)}$ and $\tilde{\alpha}^{(0,1)}$ are two functions that describes the radial and latitudinal velocity components. We have denoted them with a tilde because they are not gauge invariant. However, in the Regge-Wheeler gauge we have that $\tilde{\gamma}^{(0,1)} = \gamma^{(0,1)}$ and $\tilde{\alpha}^{(0,1)} = \alpha^{(0,1)}$, where $\gamma^{(0,1)}$ and $\alpha^{(0,1)}$ are the two polar gauge invariant velocity components [32]. When we introduce Eq. (B2) into (B1) and

calculate the integral over the 2-sphere, we obtain

$$E^{(0,1)} = \frac{1}{2} \int_0^R dr (\varepsilon + p) e^{\Phi+\Lambda} \left[r^2 \left(\tilde{\gamma}^{(0,1)} - \frac{\psi^{(0,1)}}{2} \right)^2 + \ell(\ell+1) \left(\tilde{\alpha}^{(0,1)} \right)^2 \right], \quad (\text{B3})$$

that reduces to Eq. (12) in the Regge-Wheeler gauge.

-
- [1] K. D. Kokkotas and N. Stergioulas, in *Proceedings of the 5th International Workshop: New Worlds in Astroparticle Physics, Faro, Portugal* (2005), gr-qc/0506083.
- [2] L. Baiotti, R. De Pietri, G. M. Manca, and L. Rezzolla (2006), astro-ph/0609473.
- [3] M. Saijo, T. W. Baumgarte, and S. L. Shapiro, *Astrophys. J.* **595**, 352 (2003), astro-ph/0302436.
- [4] C. D. Ott, S. Ou, J. E. Tohline, and A. Burrows, *Astrophys. J. Lett.* **625**, L119 (2005), astro-ph/0503187.
- [5] C. D. Ott, A. Burrows, L. Dessart, and E. Livne, *Phys. Rev. Lett.* **96**, 201102 (2006).
- [6] N. Stergioulas, T. A. Apostolatos, and J. A. Font, *Mon. Not. R. Astron. Soc.* **352**, 1089 (2004), astro-ph/0312648.
- [7] H. Dimmelmeier, N. Stergioulas, and J. A. Font, *Mon. Not. Roy. Astron. Soc.* **368**, 1609 (2006), astro-ph/0511394.
- [8] O. Zanotti, J. A. Font, L. Rezzolla, and P. J. Montero, *Mon. Not. R. Astron. Soc.* **356**, 1371 (2005), astro-ph/0411116.
- [9] A. Passamonti, M. Bruni, L. Gualtieri, A. Nagar, and C. F. Sopuerta, *Phys. Rev. D* **73**, 084010 (2006), gr-qc/0601001.
- [10] K. D. Kokkotas, personal communication.
- [11] LIGO, www.ligo.caltech.edu.
- [12] Adv-VIRGO, wwwcascina.virgo.infn.it/advirgo.
- [13] R. Flaminio et al., *Advanced Virgo White Paper VIR-NOT-DIR-1390-304* (2005).
- [14] B. Willke et al., *Classical Quantum Gravity* **23**, S207 (2006).
- [15] M. Bonaldi, M. Cerdonio, L. Conti, M. Pinard, G. A. Prodi, L. Taffarelli, and J. P. Zendri, *Phys. Rev. D* **68**, 102004 (2003), gr-qc/0302012.
- [16] V. V. Kovtuykh, S. M. Andrievsky, R. E. Luck, and N. I. Gorlova, *Astron. Astrophys.* **401**, 661 (2003), astro-ph/0302043.
- [17] W. A. Dziembowski and T. Mizerski, *Acta Astronomica* **54**, 363 (2004), astro-ph/0501435.
- [18] R. M. Nowakowski, *Acta Astronomica* **55**, 1 (2005), astro-ph/0501510.
- [19] K. D. Kokkotas and B. G. Schmidt, *Living Reviews in Relativity* **2**, 2 (1999).
- [20] J. A. Font, *Living Reviews in Relativity* **6**, 4 (2003).
- [21] J. A. Font, N. Stergioulas, and K. D. Kokkotas, *MNRAS* **313**, 678 (2000).
- [22] J. A. Font, H. Dimmelmeier, A. Gupta, and N. Stergioulas, *MNRAS* **325**, 1463 (2001).
- [23] J. A. Font et al., *Phys. Rev. D* **65**, 084024 (2002), gr-qc/0110047.
- [24] U. Sperhake, Ph.D. thesis, University of Southampton (2001), gr-qc/0201086.
- [25] U. Sperhake, P. Papadopoulos, and N. Andersson (2001), astro-ph/0110487.
- [26] M. Bruni, S. Matarrese, S. Mollerach, and S. Sonego, *Classical Quantum Gravity* **14**, 2585 (1997), gr-qc/9609040.
- [27] M. Bruni, L. Gualtieri, and C. F. Sopuerta, *Classical Quantum Gravity* **20**, 535 (2003), gr-qc/0207105.
- [28] C. F. Sopuerta, M. Bruni, and L. Gualtieri, *Phys. Rev. D* **70**, 064002 (2004), gr-qc/0306027.
- [29] K. Nakamura, *Progress of Theoretical Physics* **110**, 723 (2003), gr-qc/0303090.
- [30] U. H. Gerlach and U. K. Sengupta, *Phys. Rev. D* **19**, 2268 (1979).
- [31] U. H. Gerlach and U. K. Sengupta, *Phys. Rev. D* **22**, 1300 (1980).
- [32] C. Gundlach and J. M. Martín-García, *Phys. Rev. D* **61**, 084024 (2000), gr-qc/9906068.
- [33] J. M. Martín-García and C. Gundlach, *Phys. Rev. D* **64**, 024012 (2001), gr-qc/0012056.
- [34] D. Brizuela, J. M. Martín-García, and G. A. M. Marugán, *Phys. Rev. D* **74**, 044039 (2006), gr-qc/0607025.
- [35] M. Bruni, F. C. Mena, and R. K. Tavakol, *Classical Quantum Gravity* **19**, L23 (2002), gr-qc/0107069.
- [36] R. J. Gleiser, C. O. Nicasio, R. H. Price, and J. Pullin, *Classical Quantum Gravity* **13**, L117 (1996), gr-qc/9510049.
- [37] R. H. Price, in *Black Holes, Gravitational Radiation, and the Universe: Essays in Honor of C.V. Vishveshwara* (Kluwer Academic Publishers, Dordrecht, 1998), p. 351.
- [38] A. Garat and R. H. Price, *Phys. Rev. D* **61**, 044006 (2000).
- [39] M. Campanelli and C. O. Lousto, *Phys. Rev. D* **59**, 124022 (1999), gr-qc/9811019.
- [40] A. Passamonti, M. Bruni, L. Gualtieri, and C. F. Sopuerta, *Phys. Rev. D* **71**, 024022 (2005), gr-qc/0407108.
- [41] A. Passamonti, Ph.D. thesis, ICG, Porstmouth University (2006), gr-qc/0607143.
- [42] H. Dimmelmeier, J. A. Font, and E. Müller, *Astron. Astrophys.* **388**, 917 (2002).
- [43] H. Dimmelmeier, J. A. Font, and E. Müller, *Astron. Astrophys.* **393**, 523 (2002).
- [44] A. Nagar, G. Díaz, J. A. Pons, and J. A. Font, *Phys. Rev. D* **69**, 124028 (2004), gr-qc/0403077.
- [45] A. Nagar and G. Díaz, in *Proceedings of the 27th Spanish Relativity Meeting. Gravitational Radiation* (Editorial Services of the University of Alicante, Alicante, 2004).
- [46] F. J. Zerilli, *Phys. Rev. Lett.* **24**, 737 (1970).
- [47] A. Nagar and L. Rezzolla, *Classical Quantum Gravity* **23**, 4297 (2006), gr-qc/0502064.
- [48] G. Allen, N. Andersson, K. D. Kokkotas, and B. F. Schutz, *Phys. Rev. D* **58**, 124012 (1998), gr-qc/9704023.
- [49] J. Ruoff, *Phys. Rev. D* **63**, 064018 (2001).
- [50] J. M. Bardeen, K. P. Thorne, and D. W. Meltzer, *Astrophys. J.* **145**, 505 (1966).
- [51] E. Müller, M. Rampp, R. Buras, H.-T. Janka, and D. H. Shoemaker, *Astrophys. J.* **603**, 221 (2004), astro-

- ph/0309833.
- [52] C. D. Ott, H. Dimmelmeier, A. Marek, H.-T. Janka, B. Zink, I. Hawke, and E. Schnetter (2006), astro-ph/0612638.
 - [53] H. Dimmelmeier, C. D. Ott, H.-T. Janka, A. Marek, and E. Mueller (2007), astro-ph/0501435.
 - [54] É. É. Flanagan and S. A. Hughes, Phys. Rev. D **57**, 4535 (1998), gr-qc/9701039.
 - [55] EURO, www.astro.cardiff.ac.uk/geo/euro.
 - [56] N. Andersson and K. D. Kokkotas, Phys. Rev. Lett. **77**, 4134 (1996).
 - [57] K. D. Kokkotas, T. A. Apostolatos, and N. Andersson, Mon. Not. R. Astron. Soc. **320**, 307 (2001), gr-qc/9901072.
 - [58] O. Benhar, V. Ferrari, and L. Gualtieri, Phys. Rev. D **70**, 124015 (2004).
 - [59] K. D. Kokkotas and J. Ruoff, Astron. Astrophys. **366**, 565 (2001), gr-qc/0011093.
 - [60] K. S. Thorne, Astrophys. J. **158**, 1 (1969).